DINAME 2023 - Proceedings of the XIX International Symposium on Dynamic Problems of Mechanics,
A.S. De Paula, A.T. Fabro and M.R. Machado (Editors), ABCM.
Pirenópolis, Go, Brazil, February 26th to March 3rd, 2023

Analysis of Mechanical Energy Harvesters Using a Nonlinear Dynamics Perspective

Luã G. Costa, Marcelo A. Savi

Universidade Federal do Rio de Janeiro, COPPE, Department of Mechanical Engineering, Center for Nonlinear Mechanics - Mecanon, Rio de Janeiro, Brazil

Abstract: Recent technological developments are demanding for self-powered electronic systems that need wireless and portable devices. In this regard, nonlinear mechanical energy harvesting systems are proving to be a reliable solution to turn wasted environmental mechanical energy into electrical energy by means of the direct piezoelectric effect. This work addresses a numerical characterization of two mechanical energy harvesting systems investigated based on nonlinear dynamics perspective. Results show complex dynamical patterns and highlight the best application scenario for each harvester.

Keywords: Energy Harvesting, Nonlinear Dynamics, Piezoelectric Materials, Chaos, Lyapunov Exponents.

INTRODUCTION

One of the first works to suggest the concept of harness wasted vibration environmental energy to convert to useful electrical energy refers to Williams and Yates (1996), in which the authors discuss three possible forms of transduction mechanisms: piezoelectric, electromagnetic and electrostatic. Since then, an increasing number of publications deal with the topic and new transduction mechanisms were introduced in the last decade, being the magnetostrictive (Deng and Dapino, 2017) and triboelectric (Fan et al., 2012) the most common among it. Also, the exploitation of hybrid transducer mechanisms were also proposed (Halim et al., 2019). Despite the transduction mechanism, it is consensus in the literature that the introduction of nonlinearities improve the efficiency of these systems, as it can significantly enhance the frequency bandwidth of operation and the output power in several scenarios (Tran et al., 2018).

Impact-driven/non-smooth systems greatly increase the bandwidth of operation, however the larger the bandwidth, the lower is the maximum power achieved (Ai et al., 2019). In addition, it can be more susceptible to failure as those systems are heavily submitted to mechanical wear. Multistable systems are vastly employed to increase the frequency bandwidth, maintaining the power output in some cases. Yet, a multistable system implies that it has one or more potential energy barriers that need to be overcome by the system to produce efficient conversion rates (Jian et al., 2020). Bistable (Costa et al., 2021) and tristable (Kumar et al., 2017) systems are the most common class of multistable systems studied in the literature, although some works as (Zhou et al., 2017) and (Zhou et al., 2017) treated quadstable and pentastable systems, respectively. The more equilibrium points the system have, lesser can be the potential barrier of the system, making it better suitable to be applied in low-amplitude vibrations sites, but more complex to be employed. Multistable systems can also be affected by asymmetries that can enhance the performance of the harvesters (Tao-Haitao et al., 2021).

Pendulum structures can also be employed to exploit multidirectionality in the energy harvesting process, harnessing energy from multiple directions (Wu et al., 2014). Another interesting concept is the synergistic use of smart materials in the energy harvesting process to control the natural frequency of the system, widening its bandwidth of operation and retaining the maximum power output (Adeodato et al., 2021). The use of shape memory alloys together with piezoelectric materials is an alternative where a thermal energy is employed to change system properties. Quasi-Zero Stiffness systems is a new class of systems that presents a wide flat potential energy curve, which means that there is no potential energy barrier to overcome or a well to be trapped, as in multistable systems, which makes the system free to oscillate across the flat zone, increasing dramatically its bandwidth of operation (Margielewicz et al., 2022). Although promising, this system is more complex to be employed due to the specific disposal of its spring elements.

Another technique vastly employed in the literature to create additional peaks of output power is the addition of relevant degrees of freedom in the system, which makes the structure suitable to be also employed in sites with higher vibration frequencies (Tang and Yang, 2012). The addition of multiples relevant degrees of freedom can be merged with nonlinearities. Wu et al. (2014) employed a bistable element in one of the degrees of freedom of their system.

In this regard, this work addresses a numerical analysis of a generic bistable energy harvesting system, with one and two nonlinear degrees of freedom, mainly focusing on its nonlinear dynamics characteristics and performance.

PHENOMENOLOGICAL MODEL

Consider a typical 2 degrees of freedom energy harvester represented by a reduced order model presented in Fig. 1. The model can be summarized in a set of variables in which m_i is the equivalent mass, k_i is the linear stiffness, and c_i is the

viscous damping element. A piezoelectric transducer is attached to the mechanical system, being connected to a simple resistive circuit. Details of the circuit are represented in Fig. 1(b), in which $I(t)$ is the electrical current flowing through the circuit, C_p is the equivalent capacitance of the piezoelectric element, R_p and R_l are the resistance of the piezoelectric element and the load resistance, respectively. The equivalent electrical resistance of the system R is composed by these two resistances connected in parallel; θ is the electromechanical coupling of the system. The system is subjected to a harmonic external excitation of the type $z_b(t) = A\sin(\omega t)$, in which A is the excitation amplitude and ω is the excitation frequency. Finally, a duffing-type restitution force f is incorporated producing multistable characteristics, described in Eqs. 1 and 2. The values with $i = 1,2$ index represent the degree of freedom.

$$f_1(z_1) = -a_1 z_1 - b_1 z_1^3 \tag{1}$$

$$f_2(z_2 - z_1) = -a_2 (z_2 - z_1) - b_2 (z_2 - z_1)^3 \tag{2}$$

Considering a reference frequency of $\omega_0 = \sqrt{k_1/m_1}$, a dimensionless time of $\tau = \omega_0 t$, a reference length L and a reference voltage V, a normalization of the parameters is done and the dimensionless electromechanical equations of motion are represented in Eqs. 3 to 6, in which $x_1(\tau) = z_1(t)/L$, $x_2(\tau) = z_2(t)/L$, $v_1(\tau) = v_1(t)/V$ and $v_2(\tau) = v_2(t)/V$.

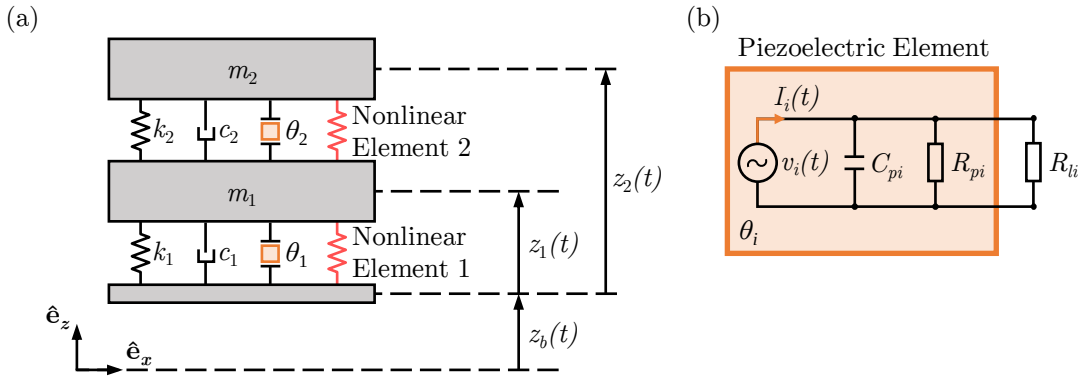

Figure 1 – Phenomenological representation of a two nonlinear degrees of freedom energy harvester. (a) Electromechanical model. (b) Circuit Representation of the transducer elements.

$$\ddot{x}_1 + 2\zeta_1\dot{x}_1 - 2\zeta_2(\dot{x}_2 - \dot{x}_1) + \alpha_1 x_1 + \beta_1 x_1^3 - \alpha_2(x_2 - x_1) - \beta_2(x_2 - x_1)^3 - \chi_1 v_1 = \gamma sin(\Omega\tau) \tag{3}$$

$$\ddot{x}_2 + (1/\rho)\left[2\zeta_2(\dot{x}_2 - \dot{x}_1) + \alpha_2(x_2 - x_1) + \beta_2(x_2 - x_1)^3 - \chi_2 v_2\right] = \gamma sin(\Omega\tau) \tag{4}$$

$$\dot{v}_1 + \varphi_1 v_1 + \kappa_1 \dot{x}_1 = 0 \tag{5}$$

$$\dot{v}_2 + \varphi_2 v_2 + \kappa_2 \dot{x}_2 = 0 \tag{6}$$

The performance of the energy harvesters can be evaluated by the RMS power measure. The Root Mean Square (RMS) of an alternate voltage can be understood as the value of the constant direct voltage that produces the same power dissipation in a resistive load. So, it can be defined as:

$$P^{\mathrm{RMS}} = \frac{1}{\tau_f - \tau_0}\int_{\tau_0}^{\tau_f}\left(\frac{\chi_1\varphi_1}{\kappa_1}v_1^2 + \frac{\chi_2\varphi_2}{\kappa_2}v_2^2\right)^2 d\tau \tag{7}$$

NUMERICAL SIMULATIONS

In this section, numerical analyses are performed focusing in 3 major aspects of the system: stability, dynamical responses and performance. Two versions of the system are analyzed: The single degree of freedom bistable energy harvester (B-EH), and the two nonlinear degrees-of-freedom energy harvester (2NDoF-EH). The parameters used in all the simulations are summarized in Tab. 1.

Stability Characteristics

The equilibrium points of both systems can be determined by the solutions of the system when both accelerations and velocities are zero in a non-forced system. The nature of stability of each solution is defined by the evaluation of the solution through a linearization of the system around each equilibrium point. Therefore, its Jacobian matrix are evaluated at each equilibrium point and by means of its eigenvalues λ^e, the stability characteristics of these points are determined. Thus, the eigenvalue spectrum of the Jacobian matrix can be classified in 3 sets: (1) Stable if $\{\lambda^e \in \mathbb{C} \mid \mathrm{Re}(\lambda^e) < 0\}$, (2) Unstable if $\{\lambda^e \in \mathbb{C} \mid \mathrm{Re}(\lambda^e) > 0\}$, and (3) Center if $\{\lambda^e \in \mathbb{C} \mid \mathrm{Re}(\lambda^e) = 0\}$. Also, the analysis can be also

Table 1 – Parameters Employed in the numerical analyses.

Single DoF Bistable Energy Harvester (B-EH)

ρ	ζ_1	ζ_2	α_1	α_2	β_1	β_2	χ_1	χ_2	φ_1	φ_2	κ_1	κ_2	Ω	γ
0	0.025	0	$-2 \rightarrow -0.25$	0	$0.25 \rightarrow 2$	0	0.05	0	0.05	0	0.5	0	$0.01 \rightarrow 3$	$0.01 \rightarrow 1$

Two Nonlinear DoF Energy Harvester (2NDoF-EH)

ρ	(ζ_1, ζ_2)	(α_1, α_2)	(β_1, β_2)	(χ_1, χ_2)	(φ_1, φ_2)	(κ_1, κ_2)	Ω	γ
1	0.025	-0.5	0.5	0.05	0.05	0.5	$0.01 \rightarrow 3$	$0.01 \rightarrow 1$

complemented by the visualization of the potential energy function of each system, determined by $U = -\int_0^X \mathfrak{f}(X)\,dX$, in which $\mathfrak{f}(X)$ is the dimensionless restitution force of the system, as X is the specific displacement of each case: $X_1 = x_1$ and $X_2 = x_2 - x_1$.

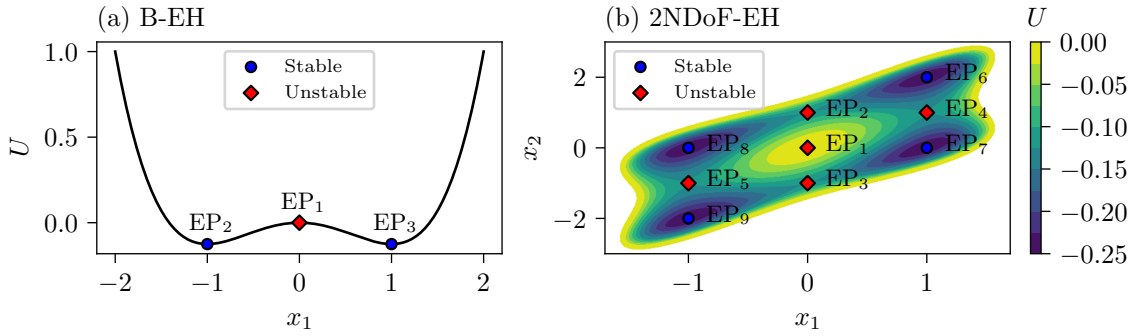

Figure 2 – Potential energy curve and equilibrium positions of (a) the B-EH system and (b) the 2NDoF-EH system. Blue dots represent stable equilibrium points, while red dots represent unstable equilibrium positions.

Figure 2 shows the stability configurations of both systems. While the B-EH have 2 stable and 1 unstable equilibrium points, the 2NDoF-EH have 4 stable and 5 unstable equilibrium points. Therefore, the addition of a single degree of freedom in the system increases the number of equilibrium points by the power of 2.

Dynamical Responses and Performance

The dynamical characteristics of the B-EH system can be evaluated by means of a dynamical response diagram, as presented in Fig. 3. The diagram is built by employing the fourth order Runge-Kutta method in a total of $n_p = 1000$ forcing periods, in order to solve the nonlinear system of electromechanical equations. Each point of the diagram is the result of a distinct integration with initial conditions based on a stable equilibrium point (in this case, EP_3 as seen in Fig. 2a). 501 x 501 samples are evaluated in order to map and identify different kinds of periodic and aperiodic attractors on a specific parameter domain (in this case, α and β). The procedure of classification of each attractor is based on the comparison of the magnitude of Lyapunov exponents and the verification of the steady state Poincaré map of the time series in each sample. Lyapunov spectrum are examined utilizing the method proposed by Wolf et al. (1985), and then compared, in two distinct initial time stages $\tau_0 = 0$ and $\tau = 0.75\tau_f$ (steady state), in order to ensure exponent convergence on samples that show long transient chaos orbits, being $\tau_f = 2\pi n_p/\Omega$ the final integration time. Results are classified based on the following attractors: Period-1 (dark gray), Period-2 (yellow), Period-3 (green), Period-4 (orange), Period-5 (purple), Period-6 or greater (light blue), Chaotic (red), Hyperchaotic (dark red).

Regarding the performance of the B-EH harvester, Fig. 4a shows the RMS power output (P^{RMS}) for the case shown in Fig. 3. To determine the best combination of restitution parameters α and β that gives high performances, 400 diagrams were compared by varying the external excitation parameters γ and Ω as shown in Tab. 1 with steps of $\Delta\gamma = 0.05$ and $\Delta\Omega = 0.1$. Also, a normalization of the type $P^{\mathrm{RMS}}_{\mathrm{norm}} = P^{\mathrm{RMS}}/P^{\mathrm{RMS}}_{\mathrm{max}}$ was done to account for the maximum and minimum power output differences in each diagram, where $P^{\mathrm{RMS}}_{\mathrm{max}}$ is the maximum power in each diagram. Figure 4b summarizes the result of this comparison for a base value of $P^{\mathrm{RMS}}_{\mathrm{norm}} = 0.5$, showing that 49.25% of the diagrams have performance greater than $P^{\mathrm{RMS}}_{\mathrm{norm}} \geq 0.5$ in the condensed region around $\alpha \approx -0.3$ and $\beta \approx 0.3$. On the other hand, Fig. 4c shows regions that shows better chances of having inter-well motion dynamics (motion that passes though two equilibrium points), which means that 91.25% of the diagrams show better bandwidths of operation around $\alpha \approx -0.4$.

The comparison between the B-EH and 2NDoF-EH on the γ and Ω parameter domain is now in focus. Fig. 5 shows the dynamical response diagrams and the power output diagrams for both systems. This time, the diagrams were built based

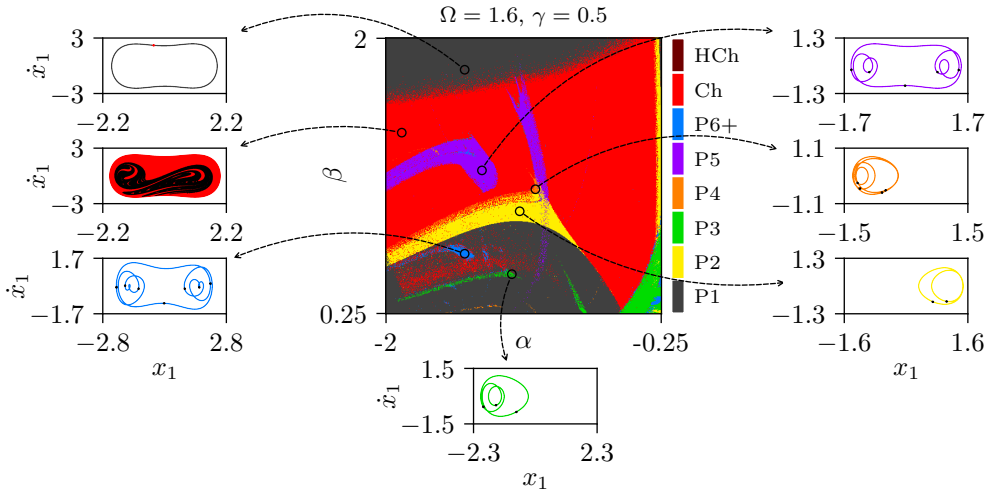

Figure 3 – Dynamical responses (attractors) for the α and β parameter domain. Each color represent a different attractor as seen in the colorbar.

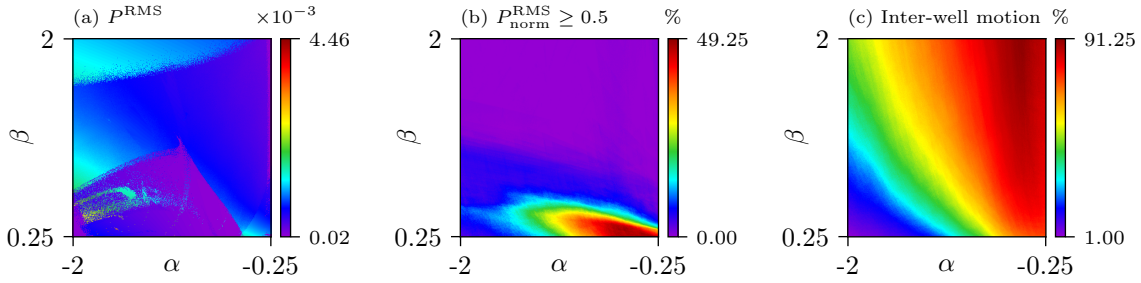

Figure 4 – Performance in the α-β domain. (a) RMS output power diagram for $\Omega = 1.6, \gamma = 0.5$. Percentage of occurrence of (b) higher values of output power and (c) inter-well motion dynamics.

on the EP_3 and EP_6 initial conditions for the B-EH and 2NDoF-EH systems, respectively. The B-EH diagram shows the predominance of period-1, period-2, period-3 and chaotic responses, while the 2NDoF-EH diagram shows greater regions of period-1 and hyperchaotic attractors. Period-2, period-4, period-6+ and chaotic are also relevant in certain concentrated spots. Regarding the performance, the output power of the 2NDoF-EH system is computed by the output power density of the system (i. e. the RMS power output divided by the number of degrees of freedom of the system: $P^{\mathrm{RMS}}_{\mathrm{2NDoF-EH}} = P^{\mathrm{RMS}}/2$). Oddly, an additional degree of freedom shortens the bandwidth and increases the maximum RMS output power density by $\approx 98.2\%$.

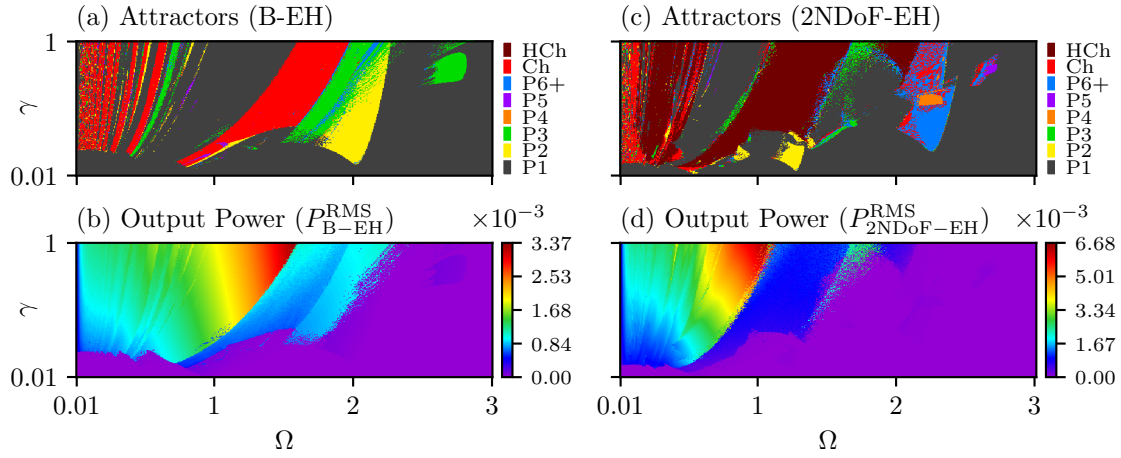

Figure 5 – Dynamical responses and RMS output power diagrams for the Ω and γ parameter domain. (a) and (b) represent the results for the B-EH system, while (c) and (d) represent the results for the 2NDoF-EH system.

CONCLUSIONS

This work deals with the analysis of two vibration energy harvesters investigating their nonlinear dynamics characteristics. The first harvester is the classic single degree of freedom bistable energy harvester (B-EH), and the second one introduces an additional degree of freedom (2NDoF-EH), which increases the number of equilibrium positions by the power of 2. Diagrams are built to evaluate the dynamical responses of both systems in two distinct sets of parameter domains: the restitution parameters $\alpha - \beta$ for the B-EH system, and the excitation parameters $\gamma - \Omega$ for the both systems. In general, systems with restitution parameters around $\alpha \approx -0.3$ and $\beta \approx 0.3$ produces more output power, while systems with $\alpha \approx -0.4$ has the tendency to have a larger bandwidth. By analyzing the external excitation parameter domain, it is shown that the B-EH presents the predominance of period-1, period-2, period-3 and chaotic solutions. On the other hand, the 2NDoF system shows the predominance period-1 and hyperchaotic solutions, with also the relevance of period-2, period-4, period-6+ and chaotic solution zones. Regarding the performance, the 2NDoF-EH shows an increase of $\approx 98.2\%$ of the output power density compared to the B-EH system. Besides, the addition of the second degree of freedom shortens the bandwidth of operation instead of increasing it. In this regard, further investigations need to be conducted in order to better explore this phenomenon.

ACKNOWLEDGMENTS

The authors would like to acknowledge the support of the Brazilian Research Agencies CNPq, CAPES and FAPERJ.

REFERENCES

Williams, C.B. and Yates, R.B. (1996) “Analysis of a Micro-Electric Generator for Microsystems”, Sensors and Actuators A: Physical, Vol.52, pp. 8-11

Deng, Z. and Dapino, M. J., 2017, “Review of magnetostrictive vibration energy harvesters”, Smart Materials and Structures, Vol.26, No. 10, pp. 103001.

Fan, F., Tian, Z. and Wang, Z. L., 2012, “Flexible triboelectric generator!”, Nano Energy, Vol.1, No. 2, pp. 328 - 334.

Tran, N., Ghayesh M. H. and Arjomandi, M., 2018, “Ambient vibration energy harvesters: A review on nonlinear techniques for performance enhancement”, International Journal of Engineering Science, Vol.127, pp.162-185.

Halim, M. A., Kabir, M. H., Cho, H. and Park, J. Y., 2019, “A Frequency up-converted hybrid energy harvester using transverse impact-driven piezoelectric bimorph for human-limb motion”, Micromachines, Vol.10, No. 10, pp. 701.

Ai, R., Monteiro, L. L. S., Monteiro Jr., P. C., Pacheco, P. M. C. L. and Savi, M. A., 2019, “Piezoelectric Vibration-Based Energy Harvesting Enhancement Exploiting Nonsmoothness”, Actuators, Vol.8, No. 1, pp. 25.

Jiang, W., Han, X., Chen, L., and Bi, Q., 2020, “Bursting vibration-based energy harvesting”, Nonlinear Dynamics, Vol.100, pp. 3043-3060.

Costa, L. G., Monteiro, L. L. S., Pacheco, P. M. C. L. and Savi, M. A., 2021, “A parametric analysis of the nonlinear dynamics of bistable vibration-based piezoelectric energy harvesters”, Journal of Intelligent Material Systems and Structures, Vol.32, No. 7, pp. 699-723.

Kumar, K. A., Ali, S. F. and Arockiarajan, A., 2017, “Magneto-elastic oscillator: Modelling and analysis with nonlinear magnetic interaction”, Journal of Sound and Vibration, Vol.393, pp. 265-284.

Zhou, Z., Qin, W. and Zhu, P., 2017, “A broadband quad-stable energy harvester and its advantaged over bi-stable harvester: Simulation and experiment verification”, Mechanical Systems and Signal Processing, Vol.84, pp.158-168.

Zhou, Z. Qin W., Yang, Y. and Zhu, P., 2017, “Improving efficiency of energy harvesting by a novel penta-stable configuration”, Sensors and Actuators A, Vol.265, pp. 297-305

Wu, Y., Qiu, J., Zhou, S., Ji, H., Chen, Y. and Li, S., 2018, “A piezoelectric spring pendulum oscillator used for multi-directional and ultra-low frequency vibration energy harvesting”, Applied Energy, Vol.231, pp. 600-614.

Adeodato, A., Duarte, B. T., Monteiro, L. L. S., Pacheco, P. M. C. L. and Savi, M. A., 2021, “Synergistic use of piezoelectric and shape memory alloy elements for vibration-based energy harvesting”, International Journal of Mechanical Sciences, Vol.194, pp. 106206.

Margielewicz, J., Gaska, D., Litak, G., Wolszczak, P., and Yurchenko, D., 2022, “Nonlinear dynamics of a new energy harvesting system with quasi-zero stiffness”, Applied Energy, Vol.307, pp. 118159.

Tao-Haitao, L., Hu, D., Xing-Jian, J., Wei-Yang, Q. and Li-Qun, C., 2021, “Improving the performance of a tri-stable energy harvester with a staircase-shaped potential well”, Mechanical Systems and Signal Processing, Vol.159, pp.107805

Tang, L. and Yang, Y., 2012, ”A multiple-degree-of-freedom piezoelectric energy harvesting model”, Journal of Intelligent Material Systems and Structures, Vol. 23, No. 14, pp. 1631–1647.

Wu, H., Tang, L., Yang, Y. and Soh, C. K., 2014, ”Development of a broadband nonlinear two-degree-of-freedom piezoelectric energy harvester”, Journal of Intelligent Material Systems and Structures, Vol. 25, No. 14, pp. 1–15.

Wolf, A., Swift, J.B., Swinney, H.L. and Vastano, J.A., 1985, “Determining Lyapunov exponents from a time series”, Physica D, Vol. 16, No. 3, pp. 285–317.

RESPONSIBILITY NOTICE

The authors are the only responsible for the printed material included in this paper.